

SCIENTIFIC REPORTS



OPEN

Growth and Deposition of Au Nanoclusters on Polymer-wrapped Graphene and Their Oxygen Reduction Activity

Received: 03 September 2014

Accepted: 21 January 2016

Published: 22 February 2016

Tsuyohiko Fujigaya^{1,2}, ChaeRin Kim¹, Yuki Hamasaki² & Naotoshi Nakashima^{1,2,3}

The development of a non-Pt electrocatalyst with a high performance for the oxygen reduction reaction (ORR) is one of the central issues in polymer electrolyte fuel cells science. Au-nanoparticles (Au-NPs) with a diameter of <2 nm are one of the promising substitutes of Pt-NPs; however, it is still a challenge to synthesize such a small-sized Au-NPs with a narrow diameter distribution on a carbon support without using capping agents. We here describe a facile method to deposit uniform Au-NPs (diameter = 1.6 nm and 3.3 nm) on the stacked-graphene (<10 layers) coated with poly[2,2'-(2,6-pyridine)-5,5'-bibenzimidazole] without using any capping agents. The obtained Au-NPs exhibit an excellent ORR activity with the onset potential at -0.11 V and -0.09 V (vs. Ag/AgCl) for 1.6 nm and 3.3 nm, respectively. On the other hand, inhomogeneous Au-NPs with 4.6 nm in average diameter shows the onset potential at -0.15 V (vs. Ag/AgCl).

Despite the inertness of bulk gold, gold nanoparticles (Au-NPs) smaller than 10 nm in diameter were recently found to exhibit a catalytic activity for reactions including the CO oxidation^{1,2} and oxygen reduction reactions (ORR)^{3–12}. The unique catalytic activity of the Au-NPs is accounted for by the enhanced adsorption of the reactant molecules on the Au-NP surfaces with a high fraction of surface atoms having low coordination numbers¹³. In particular, the Au-NPs less than 2 nm with a narrow diameter distribution loaded on the conducting supports were reported to have a high catalytic activity for the ORR^{14,15}. Thus, the Au-NPs with small diameters are considered as one of the alternative catalyst of platinum nanoparticles (Pt-NPs) that have been widely-used as fuel cell electrocatalysts owing to their remarkably high ORR activity^{16–20}. Notably, different from the Pt-based catalysts, small-sized Au-NPs were revealed to possess remarkable selectivity for the ORR with excellent tolerance to methanol oxidation^{9–11}, which means that the methanol poisoning can be ignored, which is ideal for practical applications, especially in the cathode in the direct methanol alkaline fuel cells.

Typically, small-sized Au-NPs with diameters of <2 nm with a narrow diameter distribution are synthesized in bulk solutions using a capping agents²¹. However, the capping agents on the Pt surfaces block the fuel gas access and electron transfer, which leads to serious impair their electroactivity, thereby such Au-NPs immobilized on the conducting supports show sluggish ORR reactions due to their high overpotential^{9,22,23}. In addition, due to their high surface energy, the removal of the capping agents by chemical and/or physical treatments, such as vigorous washing or thermal decomposition, has been known to causes dissolution, aggregation and sintering of the Au-NPs²⁴. To overcome these drawbacks, synthetic methods to directly grow the Au-NPs on the conducting supporting materials, such as carbon blacks (CBs), graphene oxide (GO) and carbon nanotubes (CNTs) without using a capping agent have been developed^{10,14,25}, in which the oxidized moieties, such as a carboxyl group, on the carbon materials functions as the binding and nucleation sites of the Au-NPs through the interaction between the negatively charged carboxyl group and positively charged Au ions²⁶.

Especially, GO or reduced GO (RGO) have widely been used as the supporting material of metal-NP catalysts and the RGO has been reported to induce a higher catalytic activity due to the synergetic coupling between the

¹International Institute for Carbon-Neutral Energy Research (WPI-I²CNER), Kyushu University, 744 Motooka Nishi-ku, Fukuoka 819-0395, Japan. ²Department of Applied Chemistry, Graduate School of Engineering, Kyushu University, 744 Motooka Nishi-ku, Fukuoka 819-0395, Japan. ³JST-CREST, 5 Sanbancho, Chiyoda-ku, Tokyo, 102-0075, Japan. Correspondence and requests for materials should be addressed to T.F. (email: fujigaya-tcm@mail.cstm.kyushu-u.ac.jp) or N.N. (email: nakashima-tcm@mail.cstm.kyushu-u.ac.jp)

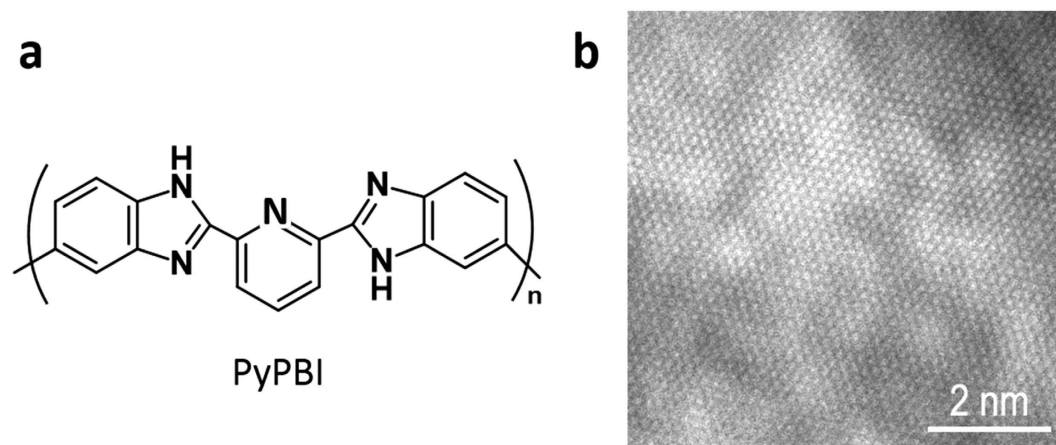


Figure 1. Structural information of PyPBI and s-Graphene/PyPBI. (a) Chemical structure of PyPBI, and (b) STEM image of the s-Graphene/PyPBI.

RGO and nanoparticles^{27–30}. Indeed, several studies preparing the small Au-NPs without using a capping agent on the RGO have been reported^{9,10,12,14,25}; however, the composites showing an excellent ORR activity are very limited due to the difficulty in synthesizing uniform small-sized Au-NPs on the supports with a narrow diameter distribution. Such difficulty might be derived from the low melting temperature of the Au-NPs⁹.

Yin *et al.* used hydrazine to reduce GO to RGO to obtain hydrazine-decollated RGO on which Au-NPs (1.8 ± 0.2 nm in diameter) with a high uniform distribution were deposited. The onset potential of the obtained catalyst showed about -0.10 V (vs. Ag/AgCl) and the corresponding current density was ~ 4.1 mAcm⁻² at -0.80 V at a 1600 rpm for O₂-saturated 0.1 M KOH solution. Very recently, Govindhan *et al.* reported a spontaneous growth of the dense dispersion of Au-NPs with an average diameter of 6.8 nm on the RGO based on the electrochemical reduction¹⁰. The Au-NPs showed onset potential of ~ -0.11 V (vs. Ag/AgCl) and the corresponding current density of ~ 2.3 mAcm⁻² at -0.4 V at a 1000 rpm under O₂-saturated 0.1 M KOH solution. However, such oxidized sites are inherently unstable in the high potential region and are readily oxidized causing corrosion, which leads to a low durability of fuel cells³¹. To avoid these crucial drawbacks, it is desirable to design and fabricate functional surfaces that enables the growth of Au-NPs with < 2 nm size with high and uniform distribution on the surfaces with highly crystalline graphitic surface.

In this study, we have developed a unique approach to create functional surfaces on the carbon surfaces based on a polymer coating, in which polybenzimidazole (PBI) was used as the polymer since we have already reported that PBI strongly adsorbs to the surfaces of pristine graphitized carbons, such as CNTs and stacked-graphene, and furthermore, they strongly bind to metal ions, such as Pt^{32–38} and Pd³⁹, through the coordination between the metal ions and PBI³⁴. The advantage of the method is that the graphitic carbon surfaces are utilized without oxidizing their carbon surfaces. In this study, we describe easy preparation of Au-NPs with ~ 3.3 nm diameter on the surfaces of pristine graphene and their oxidation reduction reaction (ORR) catalytic activities.

Results

We loaded Au-NPs using different feeding amounts of Au salt to i) explore loading efficiency, ii) to tune the size of the Au-NPs, and iii) to study their ORR activities. In this study, pristine graphene having robust two-dimensional sheets of the sp²-hybridized carbons was chosen due to its high surface area, enhanced mobility of charge carriers, and high stability^{30,40}. In our previous study, we reported that non-oxidized stacked-graphene (s-Graphene) was utilized for the loading of the Pt-NPs by the wrapping with PBI³². In this study, s-Graphene was exfoliated from graphite and wrapped with poly[2,2'-(pyridine-2,6-diyl)bibenzimidazole-5,5'-diyl] (PyPBI; Fig. 1a) in *N,N*-dimethylacetamide (DMAc) under sonication according to our previous report³². As shown in Fig. 1b, evident graphitic structure was observed in the scanning transmission electron microscopy (STEM) images. The advantage of this method is one-step non-destructive exfoliation and wrapping of s-Graphene with PyPBI that served as the binding sites of the metal ions³². The Au-NPs were then grown on the surfaces of the PyPBI-wrapped s-Graphene (s-Graphene/PyPBI) using sodium borohydride (NaBH₄) and three different concentrations (1.4, 0.7 and 0.14 mM) of chloroauric acid (HAuCl₄) as the reducing agent and Au salt, respectively (Fig. 2).

The transmission electron microscope (TEM) images of the prepared three different composites are shown in Fig. 3a,c,e from which the average diameters were determined to be 4.5 ± 1.6 , 3.3 ± 0.5 and 1.6 ± 0.3 nm, respectively (denoted as Au_{4.5}, Au_{3.3} and Au_{1.6}, respectively). Based on the TEM results, it is evident that we can control the size of the Au-NPs and Au-NCs by simply changing the feeding amounts of the Au salt (Fig. 3b,d,f). In addition, the TEM observation of the Au-NPs and Au-NCs on the s-Graphene/PyPBI at the low-magnification clearly shows homogeneous dispersion at a large area without any agglomeration, especially for Au_{3.3} and Au_{1.6} (see Supplementary Information, Fig. S1). In contrast, large particles were often observed for the Au_{4.5}. As shown in Fig. 4a,b, the high-resolution (HR) STEM images revealed that the Au_{3.3} has a highly crystalline structure with the lattice spacing of ~ 2.35 Å that corresponds to the distance of (111) as the fast Fourier-transform (FFT) analysis (see the inset of Fig. 4d)⁴¹. Of interest, in the scanning electron microscope (SEM) image, we recognized that $\sim 50\%$ of the Au_{3.3} shows a bright contrast as indicated by the white arrow, and the others showed a dark contrast

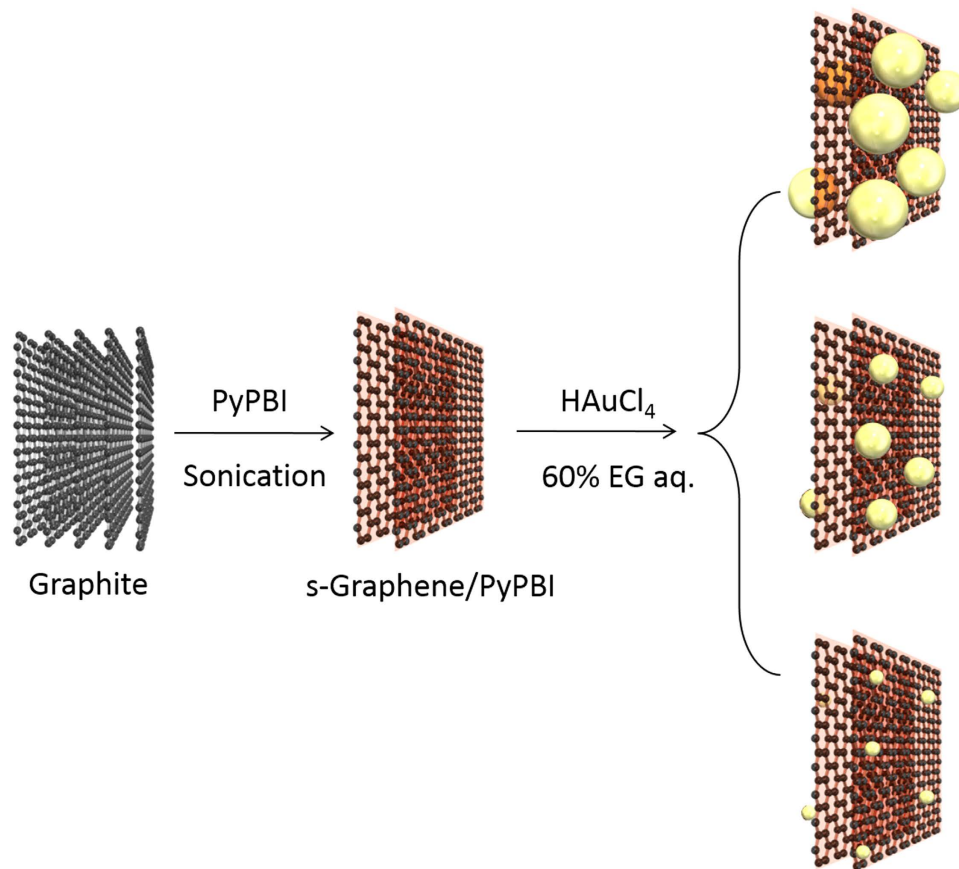


Figure 2. Schematic drawing for the preparation of the s-Graphene/PyPBI/Au_x. A series of s-Graphene/PyPBI/Au catalyst were prepared by changing the concentration of the Au salt (1.4 mM; top, 0.7 mM; middle and 0.14 mM; bottom).

indicated by the yellow arrow (Fig. 4c). By comparison with the scanning transmission electron microscopy (STEM) image in the same area (Fig. 4d), it was recognized that Au_{3,3} with the bright contrast was loaded on the front side of the s-Graphene and the others were on the back side (for the SEM and STEM images at different magnifications, see Supplementary Information, Fig. S2), which suggests that the Au_{3,3} were loaded on the surfaces of very thin s-Graphene layers.

Loaded weight % of the Au_{4,5}, Au_{3,3} and Au_{1,6} on the s-Graphene/PyPBI were determined by thermogravimetric analysis (TGA), which were 45.2, 19.2 and 8.5 wt%, respectively (Fig. 5a). In order to reveal a possible loading mechanism, the s-Graphene/PyPBI was placed in a Au salt solution not containing the reducing agent. The X-ray photoelectron spectroscopy (XPS) of the obtained material (s-Graphene/PyPBI + Au) clearly shows the binding energies at 88.6 (Au 4f 7/2) and 85.0 eV (Au 4f 5/2) that were attributed to the Au(I) (Fig. 5b)⁴². The reduction of Au(III) to Au(I) in the absence of the reducing reagent suggested that the electron transfer from the s-Graphene/PyPBI to the Au (III) ions occurred. Based on the elemental analysis using XPS, the atomic ratio (Au:N) was estimated to be 1:20. Since the theoretical ratio of Au:N was Au:N = 1:5, it was estimated that the s-Graphene/PyPBI + Au possesses one Au(I) ion per 4 PyPBI units in the absence of the reduction reagent.

We also tested the growth of Au-NPs on non-coated s-Graphene prepared by exfoliation of graphite in the absence of PyPBI at the lowest Au concentration (0.14 mM)⁴³, and recognized worm-like Au-NP structures with a broader diameter distribution (11.8 ± 6.0 nm) in the SEM images (see Supporting Information, Fig. S3). The result clearly supports that high and homogeneous dispersion of Au-NPs and Au-NCs with a small size and size distribution deposited on the carbon support is due to the anchoring effect of PyPBI.

Crystalline structure of the Au catalyst was analyzed using X-ray diffraction (XRD) measurements, and the results are shown in Fig. 6, in which we observed four diffraction peaks corresponding to the (111), (200), (220) and (311) planes in the range of 20 to 90°⁴⁴. The domain sizes (τ) of each phase were calculated using the Scherrer equation (1):

$$\tau = \frac{K\lambda}{\beta \cos \theta} \quad (1)$$

where K is the shape factor, λ is the X-ray wavelength, β is the full width at half maximum (FWHM) of the peaks, and θ is the Bragg angle. As a result, decreasing the size as decreasing of the Au concentrations were observed (see Supporting Information, Table S1). It is noted that the τ tends to become larger than the average particle size

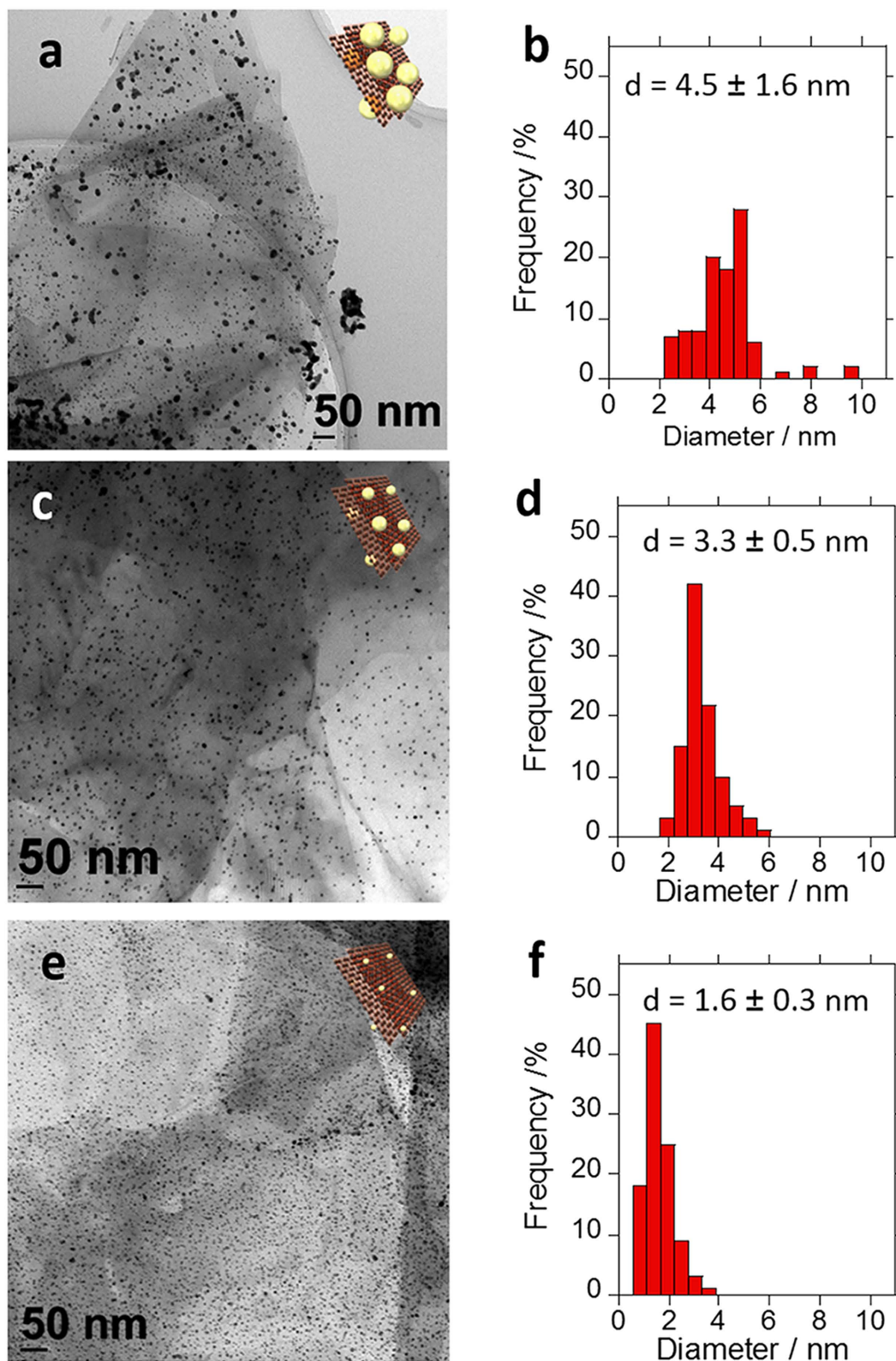


Figure 3. TEM images and the Au diameter histograms of the *s*-Graphene/PyPBI/Au catalysts. (a,c,e) TEM images of (a) *s*-Graphene/PyPBI/Au_{4.5}, (c) *s*-Graphene/PyPBI/Au_{3.3} and (e) *s*-Graphene/PyPBI/Au_{1.6}. (b,d,f) Diameter histograms of (b) *s*-Graphene/PyPBI/Au_{4.5}, (d) *s*-Graphene/PyPBI/Au_{3.3} and (f) *s*-Graphene/PyPBI/Au_{1.6} revealed the diameter of Au and density of Au loading were decreased by decreasing the feeding amount of Au salt with maintaining the homogeneous dispersion of Au on *s*-Graphene/PyPBI. (inset in a,c,e) Schematic drawing of each corresponding catalyst.

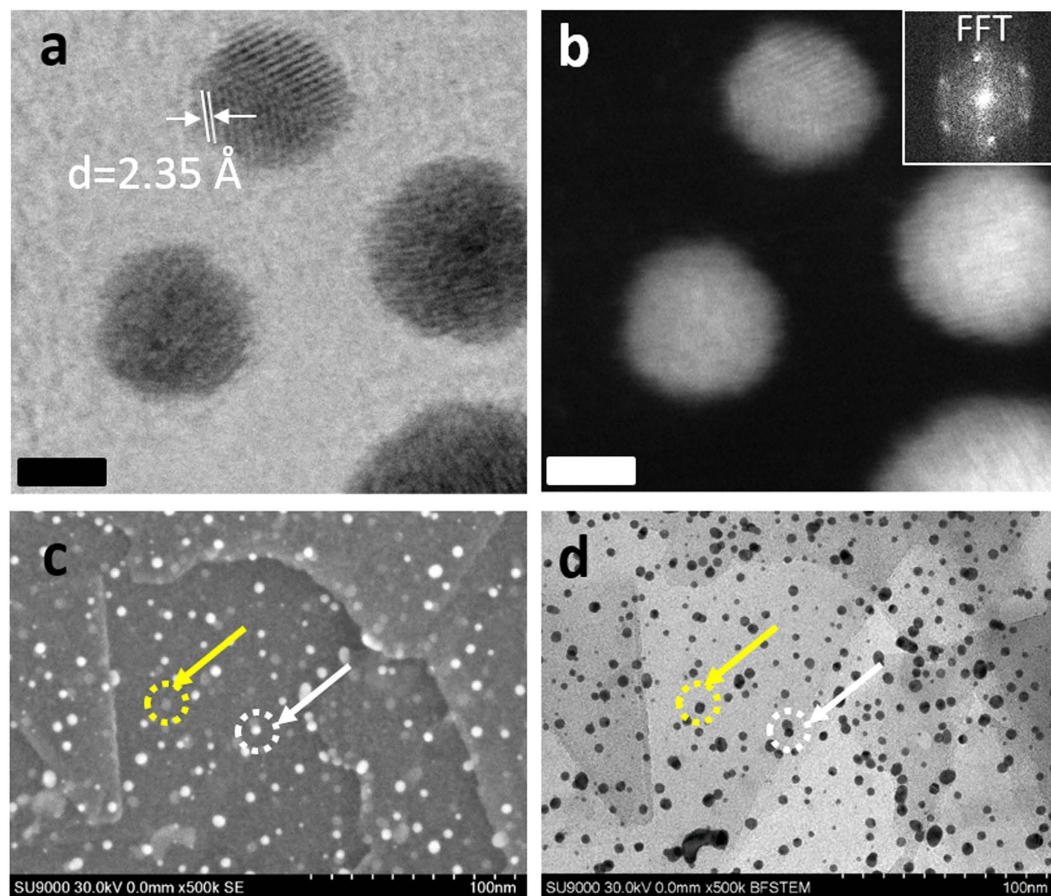


Figure 4. Electron microscope observations of Au-NP on s-Graphene/PyPBI. HR-STEM images in (a) bright-field and (b) dark-field of the Au_{3,3} show the lattice fringes for the FCC of Au. (inset) FFT pattern for the Au_{3,3}. Scale bars in a and b, 2 nm. (c) SEM and (d) STEM images of Au_{3,3}. Yellow and white circles with arrows indicate dark and bright contrast, respectively.

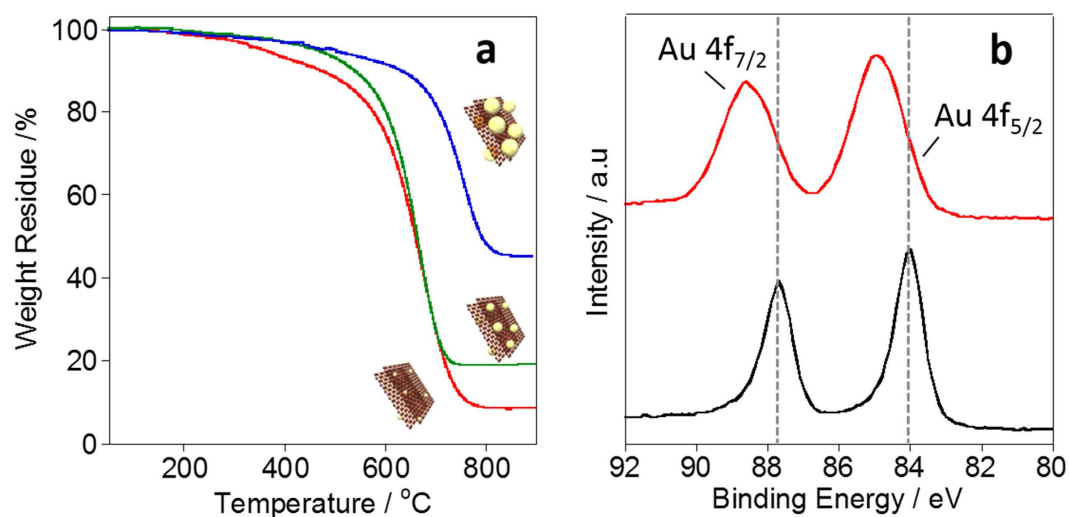


Figure 5. Characterization of the composites. (a) TGA curves of s-Graphene/PyPBI/Au_{4,5} (blue line), s-Graphene/PyPBI/Au_{3,3} (green line) and s-Graphene/PyPBI/Au_{1,6} (red line). (b) XPS narrow scans of the Au4f region for the s-Graphene/PyPBI + Au (red line) and bulk Au (black line). Indium was used as the substrate.

determined by the TEM images since, in the XRD, the signal of a large domain is accentuated and the τ is often overestimated⁴⁵. In the XPS of the Au-NPs (Fig. 7a), the Au 4f, Au 4d and N 1s are clearly observed, but the Cl 2p

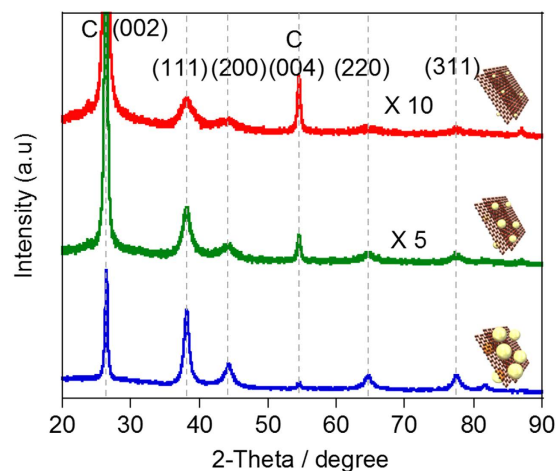


Figure 6. Analysis of the crystalline structure. (a) XRD profiles of the s-Graphene/PyPBI/Au_{4.5} (blue line), s-Graphene/PyPBI/Au_{3.3} (green line) and s-Graphene/PyPBI/Au_{1.6} (red line); (inset: schematic drawing of each corresponding catalyst).

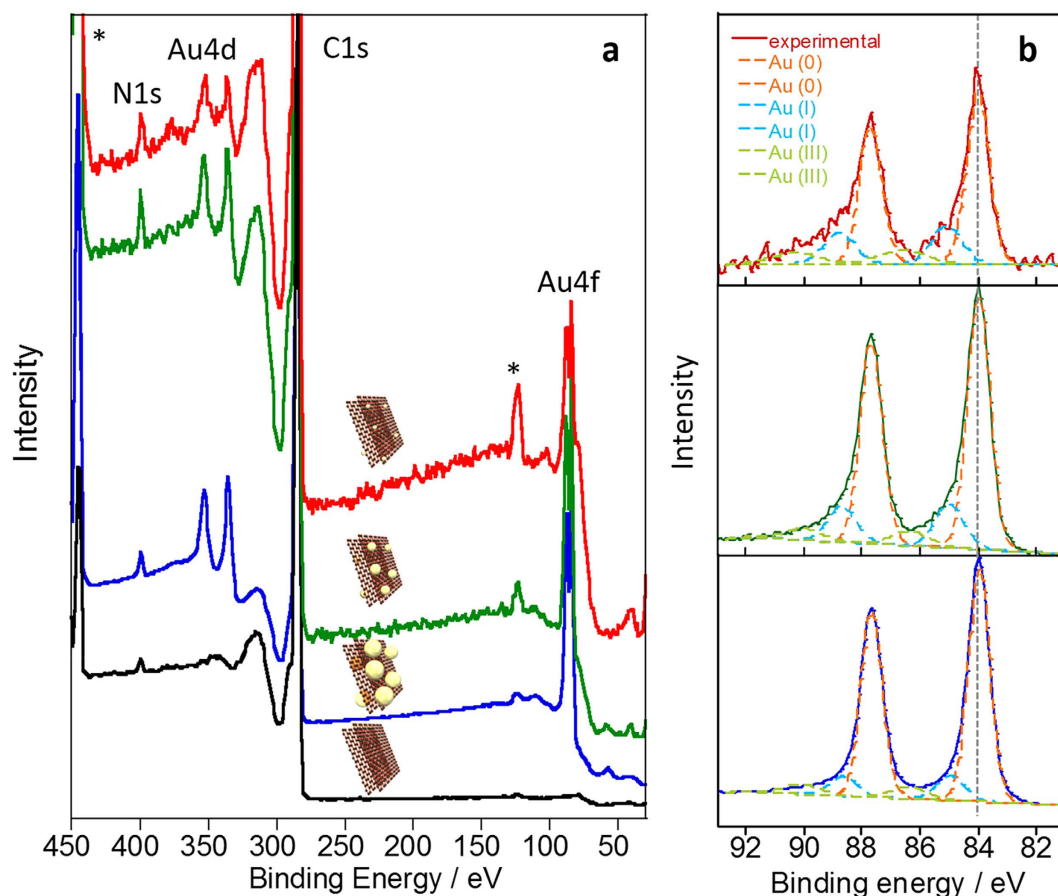


Figure 7. XPS analysis of the composites. (a) Wide and (b) narrow scans of the XPS of the s-Graphene/PyPBI/Au_{4.5} (blue line), s-Graphene/PyPBI/Au_{3.3} (green line) and s-Graphene/PyPBI/Au_{1.6} (red line). Dotted lines in b are deconvolution curves to estimate the composition ratio of Au (see Supporting Information, Table S2). Peaks with asterisk are from Indium peaks used as the substrate.

and 2s peaks at ~200 and 271 eV, respectively, were not observed, which supports the reduction of the Au. The composition ratio of the Au(0):Au(II):Au(III) were estimated by the deconvolution of the narrow scans of the Au 4f doublet (4f 7/2 and 4f 5/2) signals in the range of 83~90 eV (Fig. 7b). The composition ratio of Au(0) was found

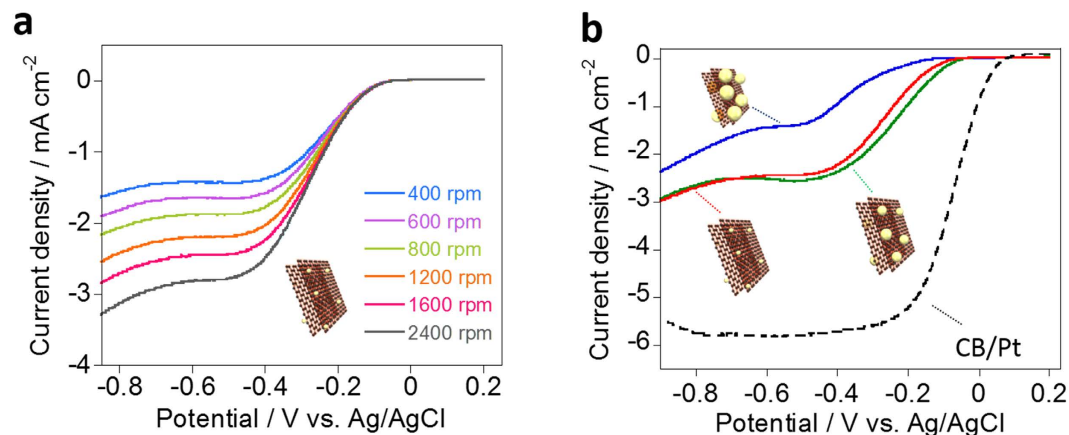


Figure 8. Electrochemical characterizations. (a) LSV curves of the s-Graphene/PyPBI/Au_{1.6} for the ORR at the given rotation rates. (b) LSV curves of the s-Graphene/PyPBI/Au_{4.5} (blue line), s-Graphene/PyPBI/Au_{3.3} (green line), s-Graphene/PyPBI/Au_{1.6} (red line) and CB/Pt (black line) measured at 1600 rpm in O₂-saturated 0.1 M KOH solutions at room temperature. Graphics of each corresponding catalyst are presented.

to be decrease as decreasing the size of the particles (see Supporting Information, Table S2). This fact is explained by the increase in the fraction of the surface atoms having low coordination numbers on the support¹³.

In order to evaluate the catalytic activity of the Au-NCs and Au-NPs, liner sweep voltammetry (LSV) measurements at the rotating speeds of 400, 600, 800, 1600 and 2400 rpm using a rotating disk electrode (RDE) were carried out in N₂- and O₂-saturated 0.1 M KOH solutions in the potential range of -0.9 – 0.2 V (vs. Ag/AgCl). Increasing the limiting current densities as increasing the rotating rates were observed for the Au_{1.6} as shown in Fig. 8a. Similar tendency was observed for both Au_{4.5} and Au_{3.3} (see the Supplementary Information, Fig. S4). As shown in Fig. 8b, the onset potentials of the ORR at 1600 rpm are -0.15 , -0.09 and -0.10 V (vs Ag/AgCl) for Au_{4.5}, Au_{3.3} and Au_{1.6}, respectively. A similar trend was reported for Au-NPs prepared by a different manner^{46–48}. Notably, the observed onset potential of -0.09 V for the Au_{3.3} is classified into the lowest overpotential ever reported (for Au-NPs on RGO, onset potential = -0.11 V vs. Ag/AgCl)¹⁰.

Discussion

As can be seen in the TEM images in Fig. 3, homogeneous Au-NCs and Au-NPs with a narrow diameter distribution were successfully deposited on the s-Graphene/PyPBI, especially for Au_{1.6} and Au_{3.3}. Such result indicated that, at a low concentration of the Au ion, Au nucleation step is significantly faster than the growth step, which leads to uniform small-sized Au nanometals, while the growth step becomes faster at a high concentration and the larger Au-NPs were formed. However, the loading efficiency of the Au nanometal were almost quantitative for all the composites (Fig. 5a). As proved in XPS (Fig. 5b), such an effective loading was realized due to the effective coordination between the benzimidazole moiety and Au ions similar to the growth mechanism of the Pt-NPs and Pd-NPs onto the PyPBI-wrapped carbon materials^{32,37,38}. Therefore, the fast nucleation step is explained by a coordination-driven mechanism. Indeed, the formation of large particles in the absence of the PyPBI-wrapping (see Fig. S3) even at the lowest concentration (0.14 mM) supported that the growth step became faster in the absence of PyPBI.

In order to consider the mechanism of the uniform and homogeneous loading of the Au-NCs and Au-NPs on the s-Graphene/PyPBI, the density of the clusters (particles) were evaluated. It was calculated that, for Au_{1.6}, Au_{3.3} and Au_{4.5}, their densities were 0.65, 0.20 and 0.06 particles/100 nm², respectively, which are much smaller than the previous report by Yin *et al.* (ca. 2.8 particles/100 nm²)⁹. Decreasing the particle density as increasing of the concentration of Au salt indicated that the growth step of the Au-NCs and Au-NPs at the higher concentrations was faster than the nucleation step. Thus, the regulation of the concentration of the Au salt is crucial to fabricate Au-NCs and Au-NPs with a small diameter with narrow diameter distribution.

In this study, both Au_{1.6} and Au_{3.3} showed a similar leveled high ORR activity (Fig. 8b), which suggested that that smaller Au-NPs is not always superior for the ORR activity. In the Koutecky-Levich (K-L) plots at various electrode potentials based on the LSV curves⁴⁶, similar trend was observed and the number of electrons for the ORR for Au_{4.5}, Au_{3.3}, and Au_{1.6} were 1.7, 2.5 and 2.4, respectively (see Supporting Information, Table S3). Such a non-linear relationship between the size of Au-NCs and Au-NP and the ORR activity was also observed in a previous literature⁹.

In conclusion, highly dispersed small and uniform Au-NCs and Au-NPs were successfully grown on the s-Graphene/PyPBI surfaces with the aid of the strong anchoring effect of the PyPBI without using any capping regents. The coating with the PyPBI enabled non-distractive modification of the surfaces of the s-Graphene as a growth sites for the Au-NCs and Au-NPs. The small Au-NCs and Au-NPs having 1.6 nm and 3.3 nm in diameter, respectively, were found to show a higher ORR activity than that of the larger Au-NPs (Au_{4.5}) probably due to a high fraction of the surface atoms having low coordination numbers.

Methods

Materials. Isopropanol, ethylene glycol (EG), DMAc, potassium hydroxide, HAuCl_4 and NaBH_4 were purchased from Wako Pure Chemical Industries, Ltd., and used as received. PyPBI was prepared according to a previous paper³⁸. Graphite (average diameter; 50 μm) was kindly provided by the Ito Graphite Co., Ltd.

Measurements. The size and distribution of the Au-NPs were measured using a TEM (JEM-2010, JEOL) at a 120-kV acceleration voltage. A copper grid with a carbon support (Okenshoji Co., Ltd.) was used for the TEM observations. Samples were dispersed in 2-propanol by an ultrasonic bath with a 10-min sonication, and a drop of the dispersion was placed on a copper grid coated with a carbon film, then dried overnight under vacuum. XRD and XPS spectra were measured using a Smart-Lab (Rigaku Corporation) and AXIS-ULTRA^{DL} (Shimadzu Corporation), respectively, in which the binding energies were calibrated using the C 1s peak that appeared at 284.5 eV. The dual monitoring by the SEM and STEM was carried out using HF-3300 (Hitachi High Technologies) and ARM-200F (JEOL) microscopes operated at the acceleration voltage of 300 kV.

Synthesis of s-Graphene/PyPBI. The mixture of graphite (30 mg) and PyPBI (30 mg) in DMAc (30 mL) was sonicated for 20 h, then mild centrifugation (500 g) was carried out to remove formed sedimented aggregates. The supernatant was then filtered using a PTFE membrane (0.2 μm pore size, Millipore) and washed with DMAc to remove any excess PyPBI. The obtained solid (s-Graphene/PyPBI) was dried overnight at 60 °C under vacuum.

Loading of Au-NPs on the s-Graphene/PyPBI. To the s-Graphene/PyPBI (5.0 mg) dispersed in 60 vol % aqueous EG (10 mL), HAuCl_4 (0.9 mg) in a 60 vol % aqueous EG solution (15 mL) and 0.1 mM of NaBH_4 (3.0 mL) in water were added. The mixture was stirred for 24 h at room temperature under N_2 . The mixture was then filtered through a PTFE filter membrane (0.1 μm pore size, Millipore), then dried overnight under vacuum to obtain three different s-Graphene/PyPBI/Au samples.

Electrochemical measurements. The electrochemical measurements were performed in a 0.1 M KOH solution at room temperature using an electrochemical analyzer (BAS, Model 2323). An Ag/AgCl and a platinum wire were used as the reference and counter electrodes, respectively. The ORR activity measurements were performed in an O_2 -saturated 0.1 M KOH solution using a rotating disk electrode (RDE) with a glassy carbon disk of 6-mm diameter. The metal loading on the GC electrodes was controlled at 5.3 $\mu\text{g}_{\text{Au}} \text{cm}^{-2}$ for all the electrochemical experiments. The data were analyzed using the Koutecky-Levich equation. This equation was used to determine the number of electrons involved in the oxygen reductions of the s-Graphene/PyPBI/Au catalysts. The kinetic parameters were calculated using the Koutecky-Levich equation which is expressed by:

$$\frac{1}{j} = \frac{1}{j_k} + \frac{1}{j_L} = \frac{1}{B\omega^{1/2}} + \frac{1}{j_k} \quad (2)$$

$$B = 0.62nFC_0D_0^{2/3}\nu^{-1/6} \quad (3)$$

$$j_k = n F k C_0 \quad (4)$$

where j is the measured current density, j_k and j_L are the kinetic and diffusion limiting current densities, respectively, ω is the electrode rotation in rad/s, n is the overall number of electrons transferred in the oxygen reduction reactions, F is the Faraday constant ($F = 96485.4 \text{ C}\cdot\text{mol}^{-1}$), C_0 is the concentration of molecular oxygen in a 0.1 M KOH solution ($C_0 = 1.2 \times 10^{-3} \text{ mol}\cdot\text{L}^{-1}$)⁴⁹, D_0 is the diffusion coefficient of O_2 ($D_0 = 1.9 \times 10^{-5} \text{ cm}^2\cdot\text{s}^{-1}$)⁴⁹, k is the electron transfer rate constant, and ν is the kinematic viscosity of the electrolyte in 0.1 M KOH ($\nu = 0.01 \text{ cm}^2 \text{ s}^{-1}$)⁵⁰.

References

- Valden, M., Lai, X. & Goodman, D. W. Onset of Catalytic Activity of Gold Clusters on Titania with the Appearance of Nonmetallic Properties. *Science* **281**, 1647–1650 (1998).
- Hayden, B. E., Pletcher, D. & Suchsland, J.-P. Enhanced Activity for Electrocatalytic Oxidation of Carbon Monoxide on Titania-Supported Gold Nanoparticles. *Angew. Chem. Int. Ed.* **46**, 3530–3532 (2007).
- Muszynski, R., Seger, B. & Kamat, P. V. Decorating Graphene Sheets with Gold Nanoparticles. *J. Phys. Chem. C* **112**, 5263–5266 (2008).
- Goncalves, G. *et al.* Surface Modification of Graphene Nanosheets with Gold Nanoparticles: The Role of Oxygen Moieties at Graphene Surface on Gold Nucleation and Growth. *Chem. Mater.* **21**, 4796–4802 (2009).
- Koo, H. Y. *et al.* Gold nanoparticle-doped graphene nanosheets: sub-nanosized gold clusters nucleate and grow at the nitrogen-induced defects on graphene surfaces. *J. Mater. Chem.* **22**, 7130–7135 (2012).
- Choi, Y. *et al.* Hybrid gold nanoparticle-reduced graphene oxide nanosheets as active catalysts for highly efficient reduction of nitroarenes. *J. Mater. Chem.* **21**, 15431–15436 (2011).
- Zhou, H. *et al.* Thickness-Dependent Morphologies of Gold on N-Layer Graphenes. *J. Am. Chem. Soc.* **132**, 944–946 (2009).
- Hong, W. *et al.* Preparation of Gold Nanoparticle/Graphene Composites with Controlled Weight Contents and Their Application in Biosensors. *J. Phys. Chem. C* **114**, 1822–1826 (2010).
- Yin, H. *et al.* Facile Synthesis of Surfactant-Free Au Cluster/Graphene Hybrids for High-Performance Oxygen Reduction Reaction. *ACS Nano* **6**, 8288–8297 (2012).
- Govindhan, M. & Chen, A. Simultaneous synthesis of gold nanoparticle/graphene nanocomposite for enhanced oxygen reduction reaction. *J. Power Sources* **274**, 928–936 (2015).
- Xu, S. & Wu, P. Facile and green synthesis of a surfactant-free Au clusters/reduced graphene oxide composite as an efficient electrocatalyst for the oxygen reduction reaction. *J. Mater. Chem. A* **2**, 13682–13690 (2014).
- Kim, S.-S., Kim, Y.-R., Chung, T. D. & Sohn, B.-H. Tunable Decoration of Reduced Graphene Oxide with Au Nanoparticles for the Oxygen Reduction Reaction. *Adv. Funct. Mater.* **24**, 2764–2771 (2014).
- Haruta, M. Size- and support-dependency in the catalysis of gold. *Catal. Today* **36**, 153–166 (1997).

14. Chen, W. & Chen, S. Oxygen Electroreduction Catalyzed by Gold Nanoclusters: Strong Core Size Effects. *Angew. Chem. Int. Ed.* **48**, 4386–4389 (2009).
15. Jayabharathi, C., Kumar, S. S., Kiruthika, G. V. M. & Phani, K. L. N. Aqueous CTAB-Assisted Electrodeposition of Gold Atomic Clusters and Their Oxygen Reduction Electrocatalytic Activity in Acid Solutions. *Angew. Chem. Int. Ed.* **49**, 2925–2928 (2010).
16. Adžić, R. R., Strbac, S. & Anastasijević, N. Electrocatalysis of oxygen on single crystal gold electrodes. *Mater. Chem. Phys.* **22**, 349–375 (1989).
17. Adžić, R. R., Tripković, A. V. & Marković, N. M. Structural effects in electrocatalysis: Oxidation of formic acid and oxygen reduction on single-crystal electrodes and the effects of foreign metal adatoms. *J. Electroanal. Chem. Interfacial Electrochem.* **150**, 79–88 (1983).
18. Hernández, J. *et al.* Characterization of the Surface Structure of Gold Nanoparticles and Nanorods Using Structure Sensitive Reactions. *J. Phys. Chem. B* **109**, 12651–12654 (2005).
19. Tang, W. *et al.* Size-Dependent Activity of Gold Nanoparticles for Oxygen Electroreduction in Alkaline Electrolyte. *J. Phys. Chem. C* **112**, 10515–10519 (2008).
20. Guo, S., Zhang, S. & Sun, S. Tuning nanoparticle catalysis for the oxygen reduction reaction. *Angew. Chem. Int. Ed.* **52**, 8526–8544 (2013).
21. Huang, X., Tan, C., Yin, Z. & Zhang, H. 25th anniversary article: Hybrid nanostructures based on two-dimensional nanomaterials. *Adv. Mater.* **26**, 2185–2203 (2014).
22. Li, D. *et al.* Surfactant Removal for Colloidal Nanoparticles from Solution Synthesis: The Effect on Catalytic Performance. *ACS Catalysis* **2**, 1358–1362 (2012).
23. Lee, Y., Loew, A. & Sun, S. Surface- and Structure-Dependent Catalytic Activity of Au Nanoparticles for Oxygen Reduction Reaction. *Chem. Mater.* **22**, 755–761 (2009).
24. Jayabharathi, C., Senthil Kumar, S., Kiruthika, G. V. M. & Phani, K. L. N. Aqueous CTAB-Assisted Electrodeposition of Gold Atomic Clusters and Their Oxygen Reduction Electrocatalytic Activity in Acid Solutions. *Angew. Chem. Int. Ed.* **49**, 2925–2928 (2010).
25. Mondal, A. & Jana, N. R. Surfactant-Free, Stable Noble Metal–Graphene Nanocomposite as High Performance Electrocatalyst. *ACS Catalysis* **4**, 593–599 (2014).
26. Huang, X., Qi, X., Boey, F. & Zhang, H. Graphene-based composites. *Chem. Soc. Rev.* **41**, 666–686 (2012).
27. Zhou, M. *et al.* Strain-Enhanced Stabilization and Catalytic Activity of Metal Nanoclusters on Graphene. *J. Phys. Chem. C* **114**, 16541–16546 (2010).
28. Lim, D.-H. & Wilcox, J. DFT-Based Study on Oxygen Adsorption on Defective Graphene-Supported Pt Nanoparticles. *J. Phys. Chem. C* **115**, 22742–22747 (2011).
29. Liang, Y. *et al.* Co₃O₄ nanocrystals on graphene as a synergistic catalyst for oxygen reduction reaction. *Nat Mater* **10**, 780–786 (2011).
30. Liu, M., Zhang, R. & Chen, W. Graphene-Supported Nanoelectrocatalysts for Fuel Cells: Synthesis, Properties, and Applications. *Chem. Rev.* **114**, 5117–5160 (2014).
31. Wang, X. *et al.* Durability investigation of carbon nanotube as catalyst support for proton exchange membrane fuel cell. *J. Power Sources* **158**, 154–159 (2006).
32. Fujigaya, T., Hirata, S. & Nakashima, N. A highly durable fuel cell electrocatalyst based on polybenzimidazole-coated stacked graphene. *J. Mater. Chem. A* **2**, 3888–3893 (2014).
33. Fujigaya, T. *et al.* Interfacial engineering of platinum catalysts for fuel cells: Methanol oxidation is dramatically improved by polymer coating on a platinum catalyst. *ChemCatChem* **5**, 1701–1704 (2013).
34. Fujigaya, T. & Nakashima, N. Fuel cell electrocatalyst using polybenzimidazole-modified carbon nanotubes as support materials. *Adv. Mater.* **25**, 1666–1681 (2013).
35. Berber, M. R., Fujigaya, T., Sasaki, K. & Nakashima, N. Remarkably Durable High Temperature Polymer Electrolyte Fuel Cell Based on Poly(vinylphosphonic acid)-doped Polybenzimidazole. *Sci. Rep.* **3**, 1764 (2013).
36. Matsumoto, K., Fujigaya, T., Sasaki, K. & Nakashima, N. Bottom-up design of carbon nanotube-based electrocatalysts and their application in high temperature operating polymer electrolyte fuel cells. *J. Mater. Chem.* **21**, 1187–1190 (2011).
37. Okamoto, M., Fujigaya, T. & Nakashima, N. Design of an Assembly of Poly(benzimidazole), Carbon Nanotubes, and Pt Nanoparticles for a Fuel-Cell Electrocatalyst with an Ideal Interfacial Nanostructure. *Small* **5**, 735–740 (2009).
38. Fujigaya, T., Okamoto, M. & Nakashima, N. Design of an assembly of pyridine-containing polybenzimidazole, carbon nanotubes and Pt nanoparticles for a fuel cell electrocatalyst with a high electrochemically active surface area. *Carbon* **47**, 3227–3232 (2009).
39. Fujigaya, T., Kim, C., Matsumoto, K. & Nakashima, N. Palladium-Based Anion-Exchange Membrane Fuel Cell Using KOH-Doped Polybenzimidazole as the Electrolyte. *ChemPlusChem* **79**, 400–405 (2014).
40. Georgakilas, V. *et al.* Functionalization of graphene: Covalent and non-covalent approaches, derivatives and applications. *Chem. Rev.* **112**, 6156–6214 (2012).
41. Xu, C., Wang, X. & Zhu, J. Graphene-Metal particle nanocomposites. *J. Phys. Chem. C* **112**, 19841–19845 (2008).
42. Kim, J., Lee, S. W., Chen, S. & Shao-Horn, Y. Synthesis and Oxygen Reduction Reaction Activity of Atomic and Nanoparticle Gold on Thiol-Functionalized Multiwall Carbon Nanotubes. *Electrochem. Solid-State Lett.* **14**, B105–B109 (2011).
43. Khan, U. *et al.* High-Concentration Solvent Exfoliation of Graphene. *Small* **6**, 864–871 (2010).
44. Sun, Z.-P., Zhang, X.-G., Liang, Y.-Y. & Li H.-L. Highly dispersed Pd nanoparticles on covalent functional MWNT surfaces for methanol oxidation in alkaline solution. *Electrochem. Commun.* **11**, 557–561 (2009).
45. Warren, B. E. *X-Ray Diffraction*. Dover Publications: New York, 1990.
46. Chen, W. & Chen, S. Oxygen electroreduction catalyzed by gold nanoclusters: Strong core size effects. *Angew. Chem. Int. Ed.* **48**, 4386–4389 (2009).
47. Lopez, N. *et al.* On the origin of the catalytic activity of gold nanoparticles for low-temperature CO oxidation. *J. Catal.* **223**, 232–235 (2004).
48. Campbell, C. T. The active site in nanoparticle gold catalysis. *Science* **306**, 234–235 (2004).
49. Davis, R. E., Horvath, G. L. & Tobias, C. W. The solubility and diffusion coefficient of oxygen in potassium hydroxide solutions. *Electrochim. Acta* **12**, 287–297 (1967).
50. Sarapu, A. *et al.* Electrochemical reduction of oxygen on nanostructured gold electrodes. *J. Electroanal. Chem.* **612**, 78–86 (2008).

Acknowledgements

The authors gratefully acknowledge Mr. H. Matsumoto and Mr. T. Sato of Hitachi High-Technologies Corporation for the measurements of the SEM/STEM dual monitoring. This study was supported in part by the project “Advanced Research Program for Energy and Environmental Technologies” commissioned by the New Energy and Industrial Technology Development Organization (NEDO), the Low-Carbon Research Network (LCnet), Grant-in-aid for JSPS Research Fellow (No. 268220 for C. K. and No. 15J04604 for Y. H.) the Ministry of Education, Culture, Sports, Science and Technology (MEXT), Japan and the Nanotechnology Platform Project (Molecules and Materials Synthesis) of the MEXT, Japan. A part of this research was supported by the Adaptable and Seamless Technology Transfer Program through Target-driven R&D, JST (AS242Z00200L) and the

Advanced Low Carbon Technology Research and Development Program (ALCA) and by The Japan Science and Technology Agency (JST) through its “Center of Innovation Science and Technology based Radical Innovation and Entrepreneurship Program (COI Program).

Author Contributions

T.F. and N.N. proposed and supervised the project. C.K. and Y.H. carried out experiments. T.F., C.K., Y.H. and N.N. wrote the manuscript.

Additional Information

Supplementary information accompanies this paper at <http://www.nature.com/srep>

Competing financial interests: The authors declare no competing financial interests.

How to cite this article: Fujigaya, T. *et al.* Growth and Deposition of Au Nanoclusters on Polymer-wrapped Graphene and Their Oxygen Reduction Activity. *Sci. Rep.* **6**, 21314; doi: 10.1038/srep21314 (2016).



This work is licensed under a Creative Commons Attribution 4.0 International License. The images or other third party material in this article are included in the article’s Creative Commons license, unless indicated otherwise in the credit line; if the material is not included under the Creative Commons license, users will need to obtain permission from the license holder to reproduce the material. To view a copy of this license, visit <http://creativecommons.org/licenses/by/4.0/>